



EXAFS-spectroscopy of mixed-valence compound YbB_{12}

Ivan Zaluzhnyy, National Research Nuclear University "MEPhI", Russia

September 7, 2011

Abstract

By the means of EXAFS spectroscopy samples of YbB_{12} were investigated. Temperature dependence of Yb -valence and the radius of the first coordination sphere of Yb were obtained. In addition, new sample holder to heat and cool samples in temperature range from -50 to 90°C was designed and tested in temperature range 20 - 80°C .

Contents

1	Introduction	3
2	Theory	3
2.1	Mixed-valence state	3
2.2	Properties of YbB_{12}	3
2.3	EXAFS equation	5
3	Experimental equipment	7
3.1	Heating sample holder	7
3.2	Beamlines A1 and C1	8
4	Measurement and data analysis	10
5	Conclusions	14

1 Introduction

During summer student program at DESY in EXAFS-spectroscopy group many tasks were completed. Three big independent parts in this work could be distinguished. First of all, new sample holder to heat and cool samples was designed for investigation of phase transition in shape memory alloy $Ti_{0.5}Ni_{0.25}Cu_{0.25}$ and new temperature control setup was tested. Then YbB_{12} -data were proceeded. Those data were obtained earlier on October 2009 and November 2010 on Doris beamline C1. And lastly the EXAFS-spectra of $Ti_{0.5}Ni_{0.25}Cu_{0.25}$ were obtained.

2 Theory

2.1 Mixed-valence state

Some elements are present in more than one oxidation state. Due to small energy splitting between two different electron states for some rare-earth elements (Ce, Eu, Sm, Tm, Yb for example) resonance

$$4f^n \rightleftharpoons 4f^{n-1} + e^-(s, d) \quad (1)$$

is possible. For single atom exact resonance is unlikely, but in solid state energy levels spreads so the probability of such processes increases (Figure 1).



Figure 1: Origin of mixed valence state

There are several ways how mixed-valence states appear. In some crystals different valence atoms can be in different crystallographic positions (Eu_3O_4). In other cases different valence atoms are in one crystallographic position, but exchange of electrons between those atoms is relatively slow and goes due to temperature (Fe_3O_4). In third case there are high-frequency electron transitions between two different valence states on each atom. The frequency of those transitions is much higher than the measuring time so one could see average non-integer valence.

2.2 Properties of YbB_{12}

Kondo insulators form an interesting class of rare earth (RE) compounds with valence instability. They behave as metals or semimetals with localized magnetic moment at

room temperatures but transform to nonmagnetic semiconductors with a narrow gap at Fermi energy on decrease of temperature. Alloys based on these systems are considered to be a perspective candidate for designing good low temperature thermoelectric materials. To create such materials it is necessary to understand the electron's states in these substances.

Kondo insulators have unique electron dispersion at low temperature. Typical disperse curve is shown on Figure 2. As one can see due to hybridization of f-shell the shape of conduction band changes and narrow gap at Fermi level appears.

Not many Kondo insulators are known presently. The most studied Kondo insulators are $FeSi$, $Ce_3Bi_4Pt_3$, SmB_6 , $CeNiSn$ and YbB_{12} . Therefore the investigation of YbB_{12} is important problem in solid state physics.

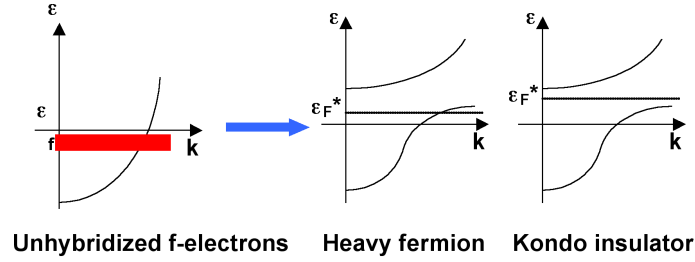


Figure 2: formation of the characteristic dispersion law for electrons [6]

Ytterbium dodecaborides (YbB_{12}) is a sample of kondo insulators. The unit cell of YbB_{12} is shown on Figure 3. The crystal structure of YbB_{12} has a NaCl-type structure (D_{2f}), where Na and Cl are corresponding to Yb and B_{12} cubo-octahedra [5]. As one can see the ytterbium atom is surrounded by 24 boron atoms. This first coordination sphere is quite stable, so one could take into account only the first summand in (3). Determination of position of other neighboring atoms by the means of EXAFS-spectroscopy seems to be very difficult and unnecessary.

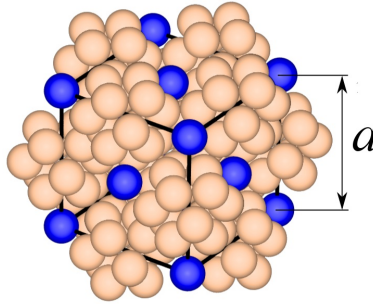


Figure 3: YbB_{12} crystal structure. The lattice constant $a = 7.469 \text{ \AA}$

2.3 EXAFS equation

Due to absorption of hard x-rays many processes are possible in matter. In Figure 4 some of those processes are shown.

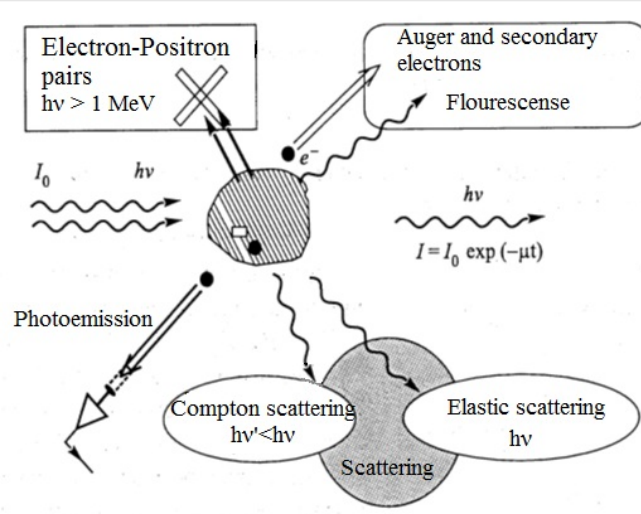


Figure 4: Possible processes in the interaction between x-ray photons and matter

The main role in interaction between x-ray photons and matter plays photoelectron process. Since energy of photon usually lies in 5-50keV range so excitation of photoelectrons from low core-levels is the most important process in EXAFS-spectroscopy. The cross section of interaction between single atom and x-ray photon depends on final state density. So cross section has a jump when the energy of photon is high enough to excite electron to new quantum state and it decreases as $1/E^3$ when photon energy is quite far from that resonance.

In case of solid state is investigated one should take into account the interaction between photoelectron and neighboring atoms. Released photoelectron is describing by a divergent spherical wave which reflects from surrounding atoms. Then incident and reflected waves interfere constructive or destructive which depends on length of photoelectron's wave vector. So for some energies of photoelectron there are permitted levels and for other energies there are forbidden quantum levels. That is the reason for absorption coefficient oscillations. These oscillations are the main subject of EXAFS spectroscopy investigation. If energy of photon is fixed the final states density depends on the interference i.e. distances between absorbing atom and its surrounding. One can extract EXAFS-oscillations $\chi(E)$ from the total absorption coefficient:

$$\chi(E) = \frac{\mu(E) - \mu_0(E)}{\mu_0(E) - \mu_b(E)} \quad (2)$$

where $\mu_0(E)$ is photoelectron absorption of single atom and $\mu_b(E)$ is absorption caused by other processes.

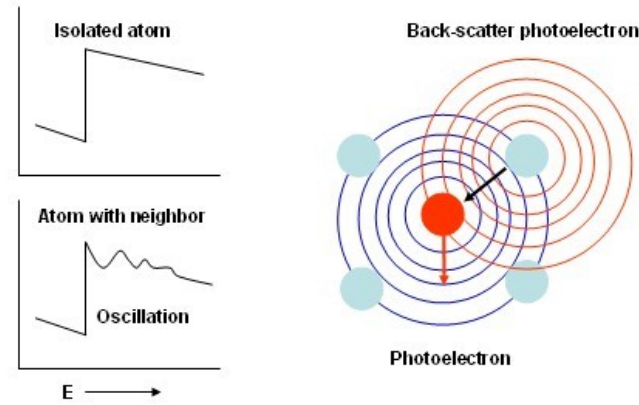


Figure 5: Origin of fine structure of EXAFS

Theoretical prediction for $\chi(k)$, where k is the wave vector of photoelectron is [1]:

$$\chi(k) = \sum_j A_j(k) \sin(2kR_j + \theta_j) \quad (3)$$

$$A_j(k) = \frac{N_j S_0^2}{k R_j^2} f_j(k) e^{-\frac{2R_j}{\lambda(k)}} e^{-2k^2 \sigma^2} \quad (4)$$

where the sum is over shells of similar neighboring atoms, R_j is the distance to neighboring atom, θ_j is a total phase shift, $f_j(k)$ is photoelectron scattering amplitude at an angle of π , $\lambda(k)$ is the photo-electrons mean free path, N_j is the number of atoms in the coordination shell, σ^2 (so-called Debye-Waller factor) is the mean square variation of distances about the average R_j , S_0^2 is a factor due to the relaxation of all the other electrons in the absorbing atom to the hole in the core level.

The function $\chi(k)$ is the sum over all coordination spheres. If R_j is big enough so summand oscillates with high frequency which can not be detected on experiment. Also amplitudes of those oscillations decrease due to factors $\frac{1}{R_j^2}$ and $e^{-\frac{2R_j}{\lambda(k)}}$. So usually one should take into account only first 1-3 spheres.

Typical way of EXAFS-experiment data analysis is fitting real $\chi(k)$ -function by equation (3) and then extracting structural parameters from fitting formula. Usually N_j is known from crystal symmetry, $f_j(k)$ is calculated by special program (FEFF, for example, [4]) so one can determine R_j , σ^2 and some other parameters from the experiment.

3 Experimental equipment

3.1 Heating sample holder

To have opportunity to measure EXAFS-spectra on different temperature (theoretically from -50°C to 90°C) special sample holder was designed. Because of the high vacuum it is impossible to use standard heating element. The old sample holder was improved and two Peltier elements were included in new model. So this model is compatible with standard liquid nitrogen cryostat used at DORIS beamlines. One can rotate and move vertically this sample holder to find the sample position.

The drawing of sample holder is on Figure 6. Peltier elements are between two metal planes. The biggest plane is attached to cryostat. On this plane there is a big hole to let the x-ray beam pass through the sample holder. In the other plane there are two places to put samples which are expected to have a shape of tablet 10mm or 13mm diameter. Also it is possible to use foils as samples. The sample should be attached to the smallest plate. Peltier elements heat the later plane and cool the cryostat which is maintained under a constant temperature. Thus one can heat the sample. On the smaller plane one should put a thermocouple to control the plane's temperature.

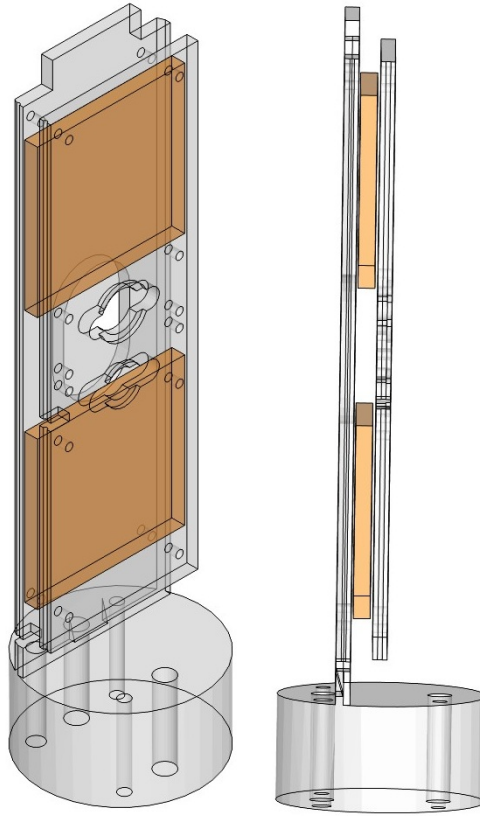


Figure 6: Sample holder. Technical drawing and sketch were made in Salome 5.1.4 [7] and 3D-Tool [8]. Orange color is used to display Peltier elements.

For this device two thermoelectric Peltier coolers were used (power 45W, voltage 12V). To control the temperature MTTC-1410 Thermoelectric Temperature Controller and PT1000 thermocouple were used.

MTTC-1410 is a bi directional controller i.e. it can heat and cool sample as well. And it can be used to control temperature in range from -100°C to 200°C and Peltier elements can maintain the temperature difference up to 70°C . If consider the cryostat temperature 20°C so one can heat or cool sample in temperature range from -50°C to 90°C . MTTC-1410 uses a Pulse Width Modulation (PWM) to provide accurate temperature control of Peltier elements.

MTTC-1410 uses a PID-logic for temperature stabilisation, so the output signal is:

$$u(t) \sim K_p e(t) + K_i \int_0^t e(t) dt + K_d \frac{\partial e(t)}{\partial t} \quad (5)$$

where $e(t)$ is the difference between set temperature and real temperature measured by thermocouple, K_p , K_i and K_d are proportional factors, t is time.

Changing the values of these proportional factors usually one can achieve temperature stability around 0.1°C . But in our case due to high vacuum heat balance of sample holder was changed, so it was necessary to find the best combination for these parameters.

The best temperature stability was achieved when $P=20$, $I=0$, $D=0$, where P , I and D are controlled parameters of MTTC-1410 which are corresponded to K_p , K_i and K_d . Also to provide the stability one should cool standard cryostat by N_2 -gas from the vessel with a liquid nitrogen. MTTC-1410 worked in proper way when the amplitude of output voltage was 3V or 7V.

Finally, we managed to maintain the sample holder temperature with 0.1°C accuracy in temperature range $10\text{-}80^{\circ}\text{C}$ for more than hour.

3.2 Beamlines A1 and C1

All data were obtained on Doris beamlines A1 and C1. Typical scheme of beamline is shown on Figure 7.

The difference between A1 and C1 beamlines is the energy range. For A1 the energy range is $2.4\text{keV} - 8.3\text{keV}$ and for C1 it is $2.4\text{keV} - 43.4\text{keV}$ [9]. So it is necessary to maintain high vacuum on A1 beamline due to high absorption of x-rays by air. New sample holder was designed to control sample temperature in vacuum.

On C1 beamline one can make experiments under the normal conditions.

During the experiment ionization currents in three chambers were measured. I_1 is proportional to intensity of x-ray beam before sample, I_2 is proportional to intensity of the beam after sample. Reference is usually well-known metal and it is used to reduce monochromator's energy drift. Energy calibration could be important when one ion type in different compounds is investigated. The pressure and type of gas in ionization chambers was selected to provide 10% absorption in the first chamber and 60% absorption in the second chamber. One can easily calculate the absorption coefficient by formula:

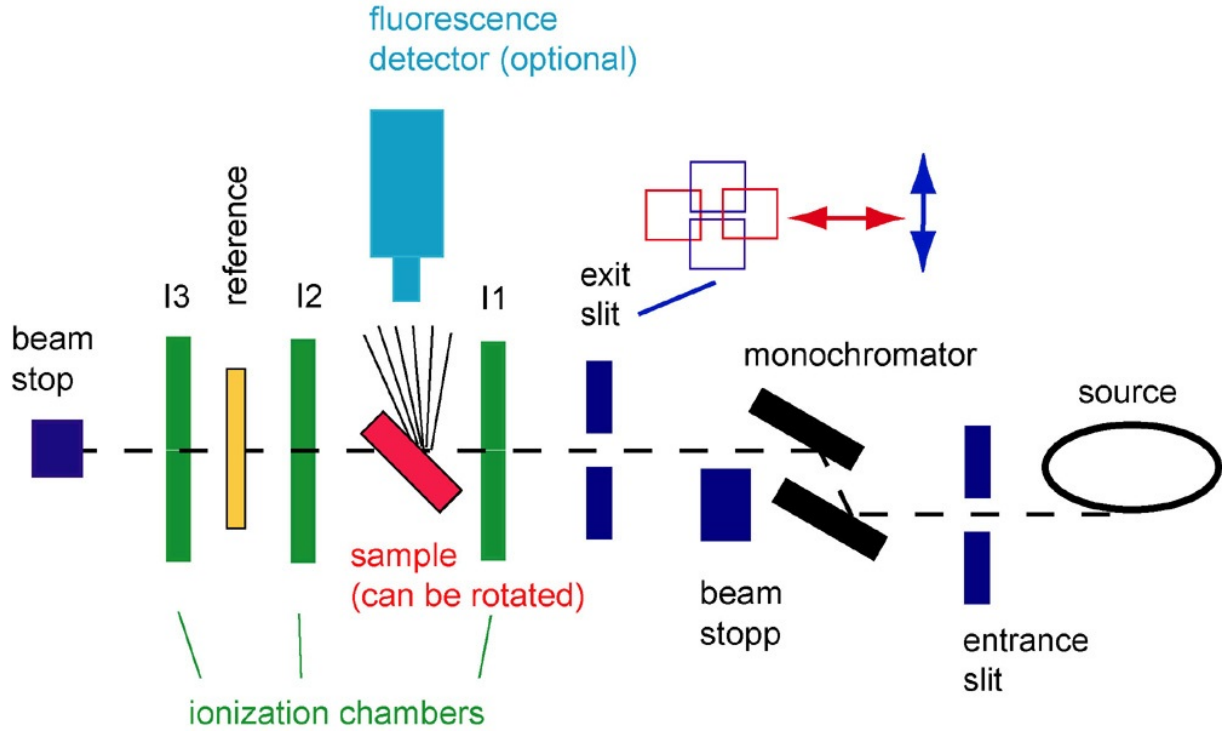


Figure 7: Beamline C1 scheme

$$\mu(E) = \frac{1}{x} \ln \frac{I_1(E)}{I_2(E)} \quad (6)$$

where x is the sample's thickness, I_1 and I_2 are currents in ionization chambers. Since ionization currents are proportional to x-ray intensity:

$$I_1 = \kappa_1 i_1, \quad I_2 = \kappa_2 i_2 \quad (7)$$

where i_1, i_2 are intensities of x-ray beam and κ_1, κ_2 are coefficients, which depend little on energy. So one can use formula 6 and take coefficients κ_1 and κ_2 into account as an additional summand to background.

4 Measurement and data analysis

Samples of YbB_{12} were investigated. EXAFS-spectra include L_{III} -edge of ytterbium. Measurements were made under wide temperature range from 5°K till 300°K so liquid helium flow cryostat was used. Typical energy dependence of absorption coefficient is represented on Figure 8.

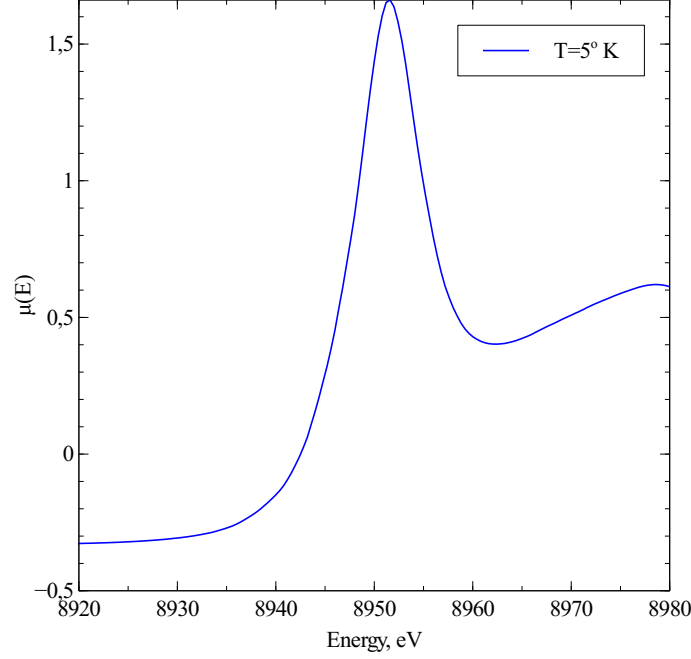


Figure 8: Absorption edge $L_{III}(Yb)$ in YbB_{12}

Then these curves (one of them is shown on Figure 8, the other curves look very similar) were fitted by function

$$f(E) = A \cdot \mu_{ref}(E - E_1) + B \cdot \mu_{ref}(E - E_2) \quad (8)$$

where $\mu_{ref}(E)$ is the absorption coefficient in $Yb_{0.8}Zr_{0.2}B_{12}$ under the room temperature. It is supposed that Yb -valence in this compound is integer ($Val(Yb) = 3$), so this function was used as a mother-function for fitting the data. In that case valence of ytterbium is

$$Val(Yb) = 2 + \frac{B}{A + B} \quad (9)$$

where A and B are determined from (8) in case $E_1 > E_2$ because left peak corresponds to lower valence state. In other case one should change A and B in formula (9). Temperature dependence of Yb -valence is shown on Figure 9. As one can see the valence of ytterbium slightly increases with temperature. It should be mentioned, that on Figure 9

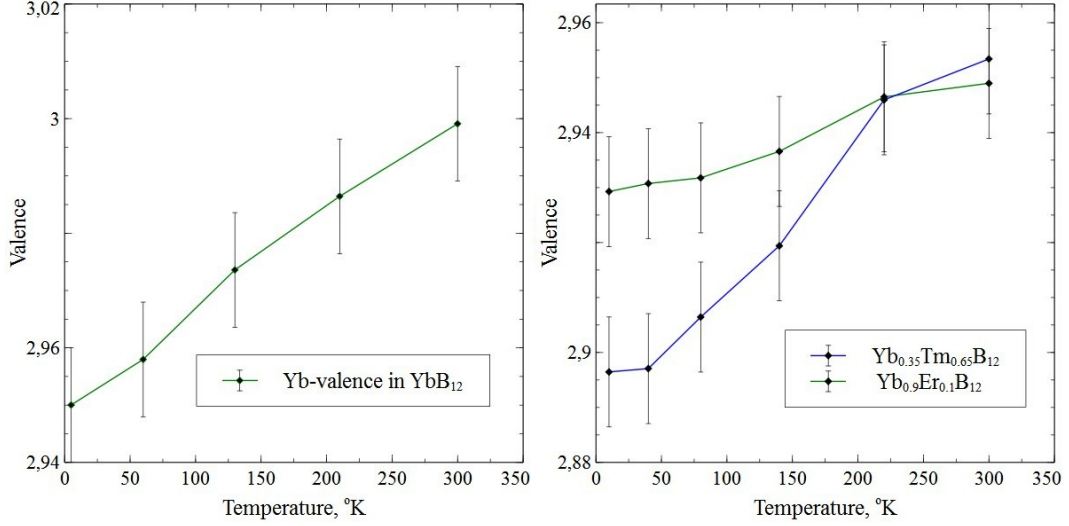


Figure 9: *Yb*-valence in YbB_{12} , $Yb_{0.35}Tm_{0.65}B_{12}$ and $Yb_{0.9}Er_{0.1}B_{12}$

and on all next figures, except Debye-Waller factors, experimental points are connected by line segments only to improve the visual perception of graphs.

Also samples of *Tm*- and *Er*-doped were investigated. The temperature dependence of *Yb*-valence is shown on Figure 9. Doping ions of *Er* and *Tm* do not change the temperature dependence of valence but they shift down the experimental points. It might be caused by high electronegativity of *Er* and *Tm* ($\chi(Yb) = 1.1, \chi(Er) = 1.24, \chi(Tm) = 1.25$ according to Pauling scale). The results for $Yb_{0.35}Tm_{0.65}B_{12}$ can not be very precise, because EXAFS-oscillations from L_{III} -edge of *Tm* change the shape of ytterbium absorption peak.

Also EXAFS-spectra of YbB_{12} were investigated. For visualization and calculations special software VIPER was used [10]. To obtain the distribution of neighboring atoms surrounding *Yb* one should make a Fourier transformation of $\chi(k)$. To amplify the EXAFS-oscillations which are far from absorption peak the function $\chi(k)$ was multiplied by k^2 . So indeed Fourier transformation of $\chi(k) \cdot k^2$ was made. One should remember that due to the phase shift in (3) the $|FT\{\chi(k) \cdot k^2\}|$ does not represent the real atoms distribution. But this graph is good enough for analysis and data fitting. Fourier transformation $|FT\{\chi(k) \cdot k^2\}|$ is shown on Figure 10.

As already mentioned only the first coordination sphere was fitted. To select the first sphere the window function $w(R)$ was used. Data fitting was made in reciprocal space. So back Fourier transformation $BFT\{|\chi(k) \cdot k^2| \cdot w(R)\}$ was made. The same transformation was made for the model and then two graphs which are shown on the right part of Figure 10 were compared.

There is the big difference in two graphs for small k -values due to inapplicability of equation (3) for small k . Then the best parameters for model were determined. Number of neighboring atoms was constant ($N = 24$), so only radius of the first coordination sphere and σ^2 were fitted.

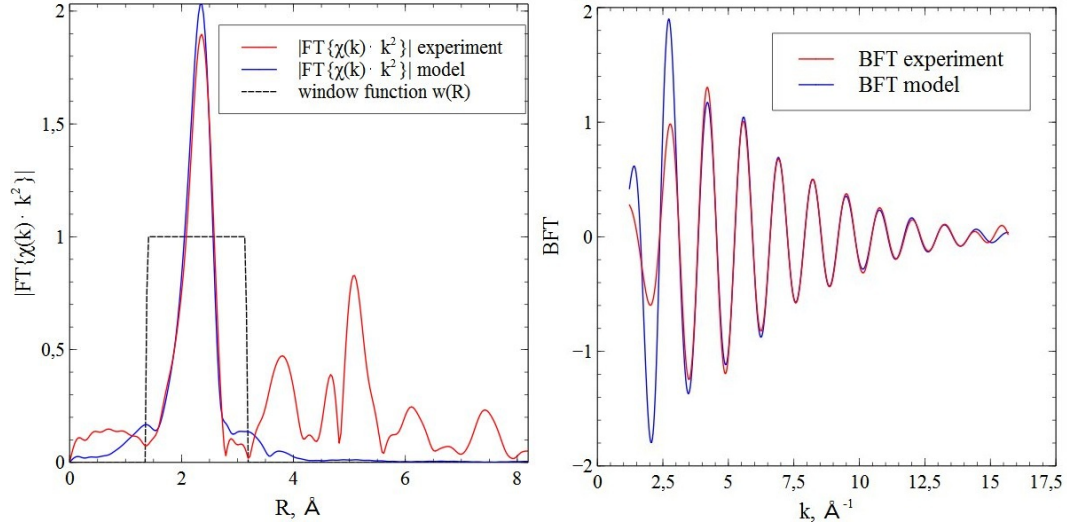


Figure 10: Model and experiment comparison

The results of data fitting are shown on Figure 11. As one can see the radius of first coordination sphere does not change within the error. It means that the shell of boron atoms is quite stable and position of ytterbium ion inside this shell does not change too. And Debye-Waller factor increases with the temperature because of displacement of atoms from lattice sites.

For Debye-Waller factor Einstein model was used. According to this approximation the Einstein temperature characterizes the stiffness of bond. Due to this model the Debye-Waller factor is given by formula:

$$\sigma^2 = \sigma_{st}^2 + \frac{\hbar^2}{2m_r k_B \theta} cth \frac{\theta}{2T} \quad (10)$$

where θ is Einstein temperature, σ_{st}^2 is static Debye-Waller factor and m_r is reduced mass.

By fitting experimental data Einstein temperature was determined. The results for YbB_{12} and other compounds are shown in Table 1.

Table 1: Einstein temperature

Compound	Einstein temperature, $^{\circ}K$
YbB_{12}	447.9
$Yb_{0.35}Tm_{0.65}B_{12}$	655.2
$Yb_{0.9}Er_{0.1}B_{12}$	467.3

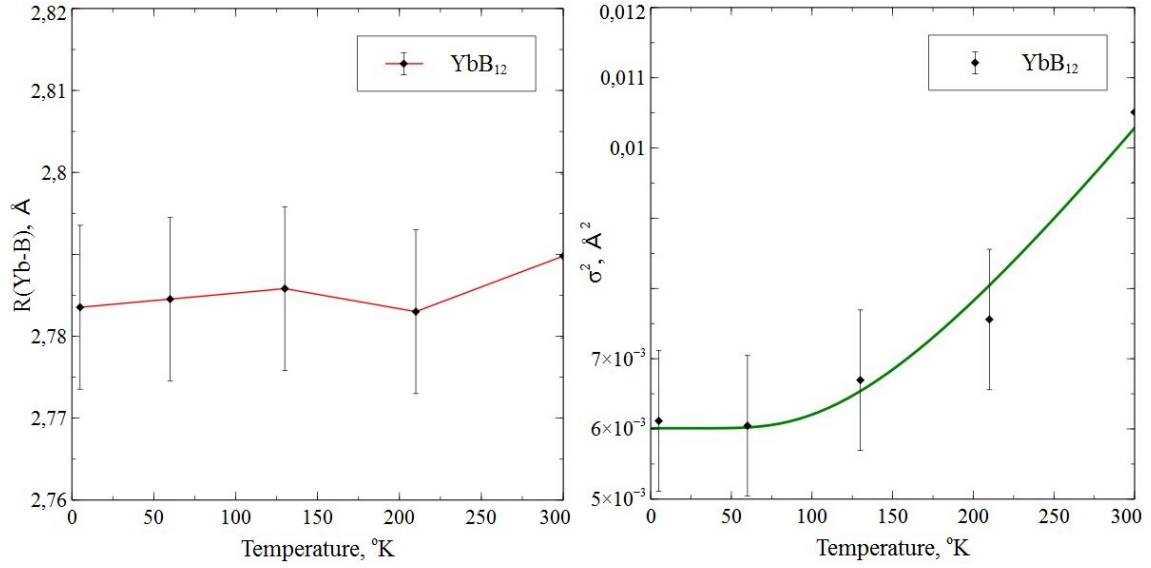


Figure 11: Temperature dependence of $\text{Yb} - \text{B}$ distance and Debye-Waller factor

The same analysis as was described above was made for $\text{Yb}_{0.35}\text{Tm}_{0.65}\text{B}_{12}$ and $\text{Yb}_{0.9}\text{Er}_{0.1}\text{B}_{12}$. On Figure 12 temperature dependence of first coordination sphere radius and Debye-Waller factor for these substances are represented.

As one can see the Einstein temperature for $\text{Yb} - \text{B}$ bond is relatively high. As mentioned above it means that the first coordination sphere is quite strong and stable. And atoms displacements due to temperature under $\sim 400^\circ\text{K}$ can not significantly change the shape of this sphere.

Due to very small value of static Debye-Waller factor and relatively big errors of fitting it was assumed equal to zero. It means that in investigated sample static displacement of Yb atoms is neglectable.

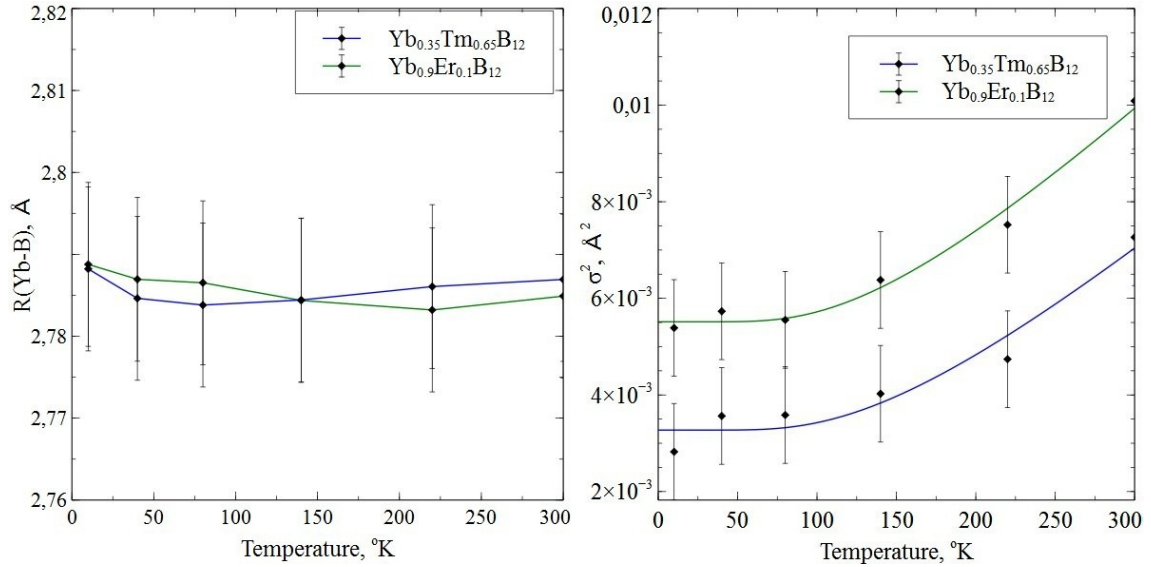


Figure 12: Temperature dependence of $\text{Yb} - \text{B}$ distance and Debye-Waller factor for $\text{Yb}_{0.35}\text{Tm}_{0.65}\text{B}_{12}$ and $\text{Yb}_{0.9}\text{Er}_{0.1}\text{B}_{12}$

5 Conclusions

During DESY summer student program samples of YbB_{12} , $Yb_{0.35}Tm_{0.65}B_{12}$ and $Yb_{0.9}Er_{0.1}B_{12}$ were investigated. Data previously obtained were proceeded. Valence of Yb in different compounds under different temperature were measured. Also analysis of EXAFS-spectra were made, so distance $Yb - B$, Debye-Waller factor and Einstein temperature were determined.

Also new sample holder to provide measuring EXAFS-spectra in vacuum at temperature range 20-80°C was designed and new temperature control system was tested.

References

- [1] Theory of the extended x-ray-absorption fine structure, Phys. Rev., B10, 8, 3027-3037, *Stern E.A.*
- [2] Introduction to XAFS: a practical guide to X-ray absorption fine structure spectroscopy, Cambridge university press, *Bunker, Grant*
- [3] Theoretical approaches to x-ray absorption fine structure, Rev. Mod. Phys., Vol. 72, No. 3, July 2000 *Rehr J.J., Albers R.C.*
- [4] Official FEFF site <http://leonardo.phys.washington.edu/feff/>
- [5] ^{171}Yb NMR in the Kondo semiconductor YbB_{12} , Physica B 281-282 (2000) 274-275 *Ikushima K., Kato Y., Takigawa M., Iga F., Hiura S., Takabatake T.*
- [6] <http://www.physics.uci.edu/faculty/fisk.html>
- [7] Official SALOME site <http://www.salome-platform.org/>
- [8] Official 3D-Tool site <http://www.3d-tool.de/english/cad-viewer.htm>
- [9] http://hasylab.desy.de/facilities/doris_iii/beamlines/index_eng.html
- [10] Official VIPER-site <http://www.cells.es/Beamlines/CLAESS/software/viper.html> *Klementiev K.*
- [11] Mixed valence properties of YbB_{12} , Journal of Magnetism and Magnetic Materials 47-48 (1985) 429-435 North-Holland, Amsterdam *Kasaya M., Iga F., Takigawa M., Kasuya T.*